LETTER

doi:10.1038/nature10840

Thresholdless nanoscale coaxial lasers

M. Khajavikhan[1], A. Simic[1]*, M. Katz[1]*, J. H. Lee[1]†, B. Slutsky[1], A. Mizrahi[1], V. Lomakin[1] & Y. Fainman[1]

The effects of cavity quantum electrodynamics (QED), caused by the interaction of matter and the electromagnetic field in subwavelength resonant structures, have been the subject of intense research in recent years[1]. The generation of coherent radiation by subwavelength resonant structures has attracted considerable interest, not only as a means of exploring the QED effects that emerge at small volume, but also for its potential in applications ranging from on-chip optical communication to ultrahigh-resolution and high-throughput imaging, sensing and spectroscopy. One such strand of research is aimed at developing the 'ultimate' nanolaser: a scalable, low-threshold, efficient source of radiation that operates at room temperature and occupies a small volume on a chip[2]. Different resonators have been proposed for the realization of such a nanolaser—microdisk[3] and photonic bandgap[4] resonators, and, more recently, metallic[5,6], metallo-dielectric[7–10] and plasmonic[11,12] resonators. But progress towards realizing the ultimate nanolaser has been hindered by the lack of a systematic approach to scaling down the size of the laser cavity without significantly increasing the threshold power required for lasing. Here we describe a family of coaxial nanostructured cavities that potentially solve the resonator scalability challenge by means of their geometry and metal composition. Using these coaxial nanocavities, we demonstrate the smallest room-temperature, continuous-wave telecommunications-frequency laser to date. In addition, by further modifying the design of these coaxial nanocavities, we achieve thresholdless lasing with a broadband gain medium. In addition to enabling laser applications, these nanoscale resonators should provide a powerful platform for the development of other QED devices and metamaterials in which atom–field interactions generate new functionalities[13,14].

The miniaturization of laser resonators using dielectric or metallic material structures faces two challenges: (1) the (eigen-)mode scalability, implying the existence of a self-sustained electromagnetic field regardless of the cavity size, and (2) a relationship between optical gain and cavity loss which results in a large and/or unattainable lasing threshold as the volume of the resonator is reduced[15]. Here we propose and demonstrate a new approach to nano-cavity design that resolves both challenges: first, subwavelength-size nano-cavities with modes far smaller than the operating wavelength are realized by designing a plasmonic coaxial resonator that supports the cut-off-free transverse electromagnetic (TEM) mode; second, the high lasing threshold for small resonators is reduced by utilizing cavity QED effects, causing high coupling of spontaneous emission into the lasing mode[16,17]. When fully exploited, this approach can completely eliminate the threshold constraint by reaching so-called thresholdless lasing, which occurs when every photon emitted by the gain medium is funnelled into the lasing mode[16,17].

The coaxial laser cavity is shown in Fig. 1a. At the heart of the cavity lies a coaxial waveguide that supports plasmonic modes and is composed of a metallic rod enclosed by a metal-coated semiconductor ring[18,19]. The impedance mismatch between a free-standing coaxial waveguide and free space creates a resonator. However, our design uses additional metal coverage on top of the device and thin, low-index dielectric plugs of silicon dioxide (SiO_2) at the top end of the coaxial waveguide and air at the bottom end to improve the mode confinement. The role of the top SiO_2 plug is to prevent the formation of undesirable plasmonic modes at the top interface, between the metal and the gain medium. The lower air plug is used to allow pump energy into the cavity and also to couple out the light generated in the coaxial resonator. The metal in the sidewalls of the coaxial cavity is placed in direct contact with the semiconductor to ensure the support of plasmonic modes, providing a large overlap between the modes of the resonator and the emitters distributed in the volume of the gain medium. In addition, the metallic coating serves as a heat sink that facilitates room-temperature and continuous-wave operation.

To reduce the lasing threshold, the coaxial structures are designed to maximize the benefits from the modification of the spontaneous emission due to the cavity QED effects[16,17]. Because of their small size, the modal content of the nanoscale coaxial cavities is sparse, which is a key requirement to obtain high spontaneous emission coupling into the lasing mode of the resonator. Their modal content can be further modified by tailoring the geometry, that is, the radius of the core, the width of the ring, and the height of the gain medium and the low-index plugs. Note that the number of modes supported by the

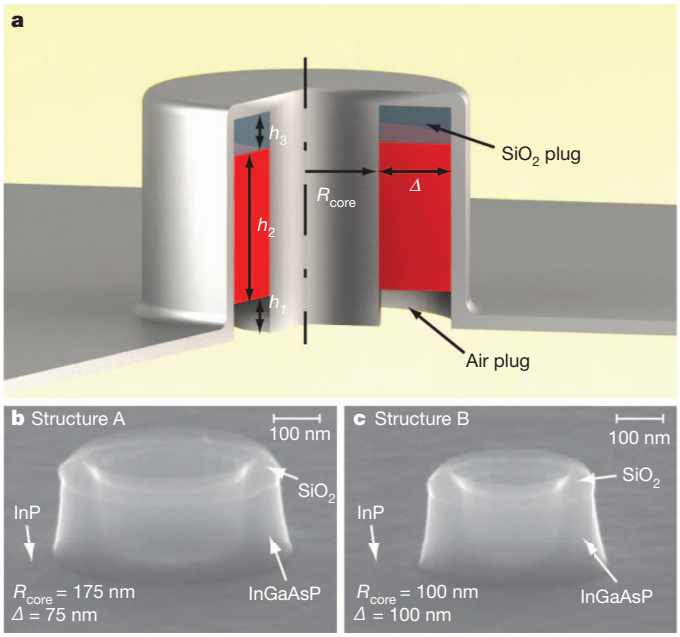

Figure 1 | Nanoscale coaxial laser cavity. a, Diagram of a coaxial laser cavity; the gain medium is shown in red. See main text for description of nomenclature. **b**, **c**, Scanning electron microscope images of the constituent rings in structure A and structure B, respectively. A side view of the rings comprising the coaxial structures is seen; the rings consist of SiO_2 on top, and a quantum-well gain region underneath. See main text for details.

[1]Department of Electrical and Computer Engineering, University of California San Diego, 9500 Gilman Drive, La Jolla, California 92093-0407, USA. †Present address: Oracle Labs, 9515 Town Centre Drive, San Diego, California 92121, USA.
*These authors contributed equally to this work.

resonator that can participate in the lasing process is ultimately limited to those that occur at frequencies that coincide with the gain bandwidth of the semiconductor gain material. In this work we use a semiconductor gain medium composed of six quantum wells of $In_{x=0.56}Ga_{1-x}As_{y=0.938}P_{1-y}$ (10 nm thick)/$In_{x=0.734}Ga_{1-x}As_{y=0.57}P_{1-y}$ (20 nm thick), resulting in a gain bandwidth that spans frequencies corresponding to wavelengths in vacuum from 1.26 μm to 1.59 μm at room temperature (295 K), and from 1.27 μm to 1.53 μm at a temperature of 4.5 K (ref. 20).

We consider two different geometries of the structure shown in Fig. 1a. The first, referred to as structure A, has an inner core radius of $R_{core} = 175$ nm, a gain-medium ring with a thickness of $\Delta = 75$ nm, a lower plug height of $h_1 = 20$ nm, a quantum-wells height of 200 nm covered by a 10-nm overlayer of InP, resulting in a total gain-medium height of $h_2 = 210$ nm, and an upper plug height of $h_3 = 30$ nm. The second, structure B, is smaller in diameter, having $R_{core} = 100$ nm and $\Delta = 100$ nm. The heights of the plugs and gain medium are identical to those of structure A. Figure 1b and c shows scanning electron microscope images of the constituent rings in structure A and structure B, respectively. The two structures are fabricated using standard nanofabrication techniques. Additional details of the fabrication procedure are provided in Supplementary Information part 1.

Figure 2 shows the modal content of the two structures at a temperature of 4.5 K, modelled using the three-dimensional finite element method (FEM) eigenfrequency solver in the radio-frequency package of COMSOL Multiphysics. Figure 2a shows that for structure A the fundamental TEM-like mode and the two degenerate HE_{11} modes are supported by the resonator and fall within the gain bandwidth of the gain material. This simulation is also repeated for structure A with room-temperature material parameters (see Supplementary Fig. 1), showing that for structure A at room temperature, the two degenerate HE_{11} modes are red-shifted to 1,400 nm, and exhibit a reduced quality factor of $Q \approx 35$, compared to $Q \approx 47$ at 4.5 K. The TEM-like mode is red-shifted to 1,520 nm with $Q \approx 53$, compared to $Q \approx 120$ at 4.5 K. All cavity quality factors are at transparency, meaning that the imaginary part of the gain medium's permittivity is set to zero in the calculations. The simulations are performed with nominal values for the permittivity of the active medium and metal at 4.5 K and at room temperature (see Supplementary Information part 2). A discussion on deviations of the material properties from nominal values, as well as additional technical details about FEM simulations, are provided in Supplementary Information part 3.

Structure B, shown in Fig. 2b, supports only the fundamental TEM-like mode at a temperature of 4.5 K. The quality factor $Q \approx 265$ for this mode is higher than that of structure A. In general, the metal coating and the small aperture of the nanoscale coaxial cavity inhibit the gain emitters from coupling into the continuum of the free-space radiation modes[21]. Hence, the single-mode cavity of structure B exhibits a very high spontaneous emission coupling factor ($\beta \approx 0.99$), approaching the condition for an ideal thresholdless laser[16,17]. The spontaneous emission factor is calculated by placing randomly oriented and randomly positioned dipoles in the active area of the cavity, and then computing their emitted power at different wavelengths. The β-factor is given by the emitted power that spectrally coincides with the lasing mode, divided by the total emitted power[22].

Characterization of the nanoscale coaxial lasers was performed under optical pumping with a $\lambda = 1{,}064$ nm laser pump beam in continuous wave and pulsed regime. Additional details on the measurement system are provided in Supplementary Information part 4. Excitation of the cavity modes is confirmed by the measurements of the far-field emission from the devices. The mode profiles are given in Supplementary Information part 5.

Figure 3 shows the emission characteristics of the nanoscale coaxial laser of structure A operating at 4.5 K (light–light curve, Fig. 3a; spectral evolution, Fig. 3b; linewidth, Fig. 3c) and at room temperature (light–light curve, Fig. 3d; spectral evolution, Fig. 3e; linewidth, Fig. 3f). The light–light curves of Fig. 3a and d show standard laser action behaviour, where spontaneous emission dominates at lower pump powers (referred to as the photoluminescence region), and stimulated emission is dominant at higher pump powers (referred to as the lasing region). The photoluminescence and lasing regions are connected through a pronounced transient region, referred to as amplified spontaneous emission (ASE). The evolution of the spectrum shown in Fig. 3b and e also confirms these three regimes of operation. The spectral profiles at low pump powers reflect the modification of the spontaneous emission spectrum by the cavity resonances depicted in Fig. 2a. The linewidth of the lasers shown in Fig. 3c and f narrows with the inverse of the output power at lower pump levels (the solid trend line). This is in agreement with the well-known Schawlow–Townes formula for lasers operating below threshold[23]. Around threshold, in semiconductor lasers the rapid increase of the coupling between the gain coefficient and the refractive index of the gain medium slows down the narrowing of the linewidth, until charge carrier pinning resumes the modified Schawlow–Townes inverse power narrowing rate[24,25]. In practice, only a few semiconductor lasers are shown to have above-threshold linewidth behaviour that follows the modified Schawlow–Townes formula. In most reported lasers, the linewidth behaviour differs distinctly from the inverse power narrowing rate. The mechanisms affecting the above-threshold linewidth, especially for lasers with high spontaneous emission coupling to the lasing mode, are still a subject of research[26–28]. Supplementary Information part 6 contains detailed diagrams of emission properties for the lasers reported above.

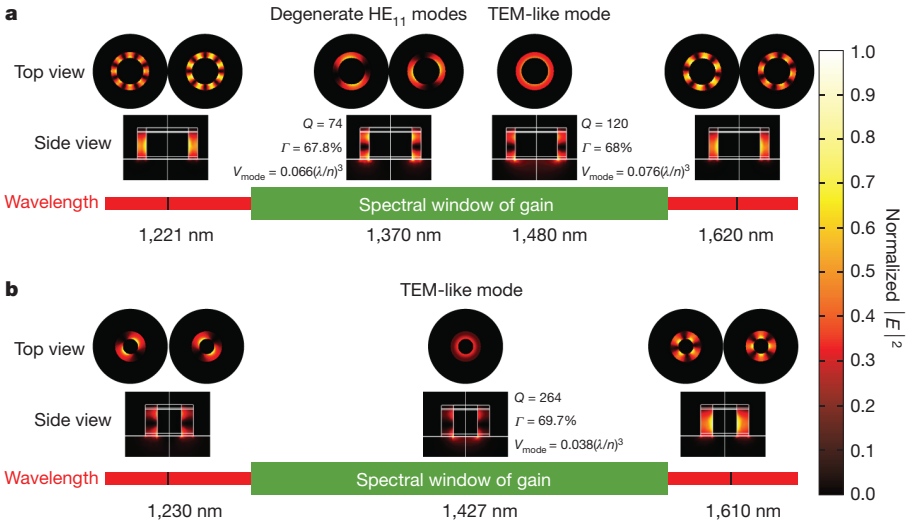

Figure 2 | Simulation of the electromagnetic properties of nanoscale coaxial cavities. **a**, The modal spectrum of the cavity of structure A at a temperature of 4.5 K. **b**, As **a** but for structure B. Q, quality factor; Γ, factor giving extent of energy confinement to the semiconductor region[30]; V_{mode}, the effective modal volume[30]. The colour bar shows normalized $|E|^2$, where E is the electric field intensity. Nominal permittivity values are used in this simulation. (See Supplementary Information parts 2 and 3 for nominal permittivities and the deviation of the permittivities from the nominal values, respectively.)

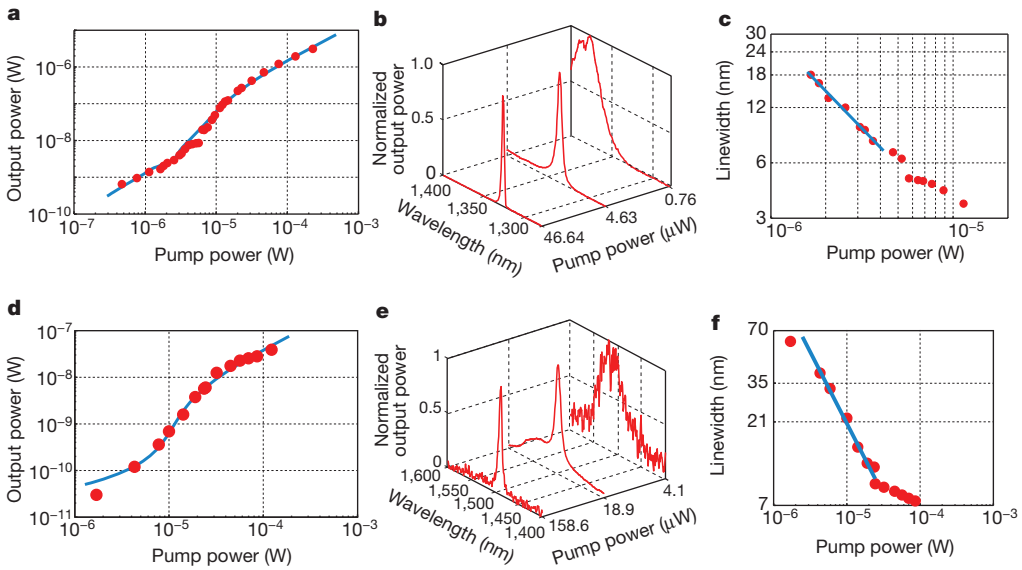

Figure 3 | Optical characterization of nanoscale coaxial cavities of structure A at 4.5 K and room temperature, showing lasing. **a**–**c**, At 4.5 K; **d**–**f**, at room temperature. Shown are light–light curves (**a**, **d**), spectral evolution diagrams for lasers with threshold (**b**, **e**), and linewidth versus pump power (**c**, **f**). The pump power is calculated as the fraction of the power incident on the laser aperture. The solid curves in **a** and **d** are the best fit of the rate-equation model. The solid lines in **c** and **f** show the inverse power narrowing rate of the linewidth. The resolution of the monochromator was set to 3.3 nm.

A rate-equation model is adopted to study the dynamics of the photon–carriers interaction in the laser cavities. Details of the rate-equation model are provided in Supplementary Information part 7. The light–light curves obtained from the rate-equation model for the laser of structure A are shown as solid blue lines in Fig. 3a and d. For the laser operating at 4.5 K, by fitting the rate-equation model to the experimental data, we found that almost 20% of the spontaneous emission is coupled to the lasing mode, which is assumed to be the mode with the highest quality factor (TEM-like mode). This assumption is validated by examining the far-field radiation pattern and the polarization state of the output beam (see Supplementary Information part 5). At room temperature, the surface and Auger non-radiative recombination processes dominate. As the carriers are lost through non-radiative channels, the ASE kink of the laser is more pronounced, and, as expected, the laser threshold shifts to higher pump powers.

Next, we examine the emission characteristics of structure B. According to the electromagnetic analysis (Fig. 2b), this structure is expected to operate as a thresholdless laser, as only one non-degenerate mode resides within the gain medium's emission bandwidth. The emission characteristics of structure B at 4.5 K are shown in Fig. 4. More detailed diagrams of emission properties for this laser are also given in Supplementary Information part 6. The light–light curve of Fig. 4a, which follows a straight line with no pronounced kink, agrees with the thresholdless lasing hypothesis. The thresholdless behaviour is further manifested in the spectral evolution, seen in Fig. 4b, where a single narrow, Lorentzian-like emission is obtained over the entire five-orders-of-magnitude range of pump power. This range spans from the first signal detected above the detection system noise floor at 720 pW pump power, to the highest pump power of more than 100 μW. Because the homogeneously broadened linewidth of the gain medium is larger than the linewidth of the observed emission, the emission profile is attributed to the cavity mode. The measured linewidth at low pump power ($\Delta\lambda_{FWHM} \approx 5$ nm), which agrees with the cavity Q-factor of the TEM-like mode at transparency, as well as the radiation pattern reported in Supplementary Information part 5, confirm the electromagnetic simulation given in Fig. 2b.

The assertion that the device indeed reaches lasing is further substantiated by careful study of the linewidth behaviour. At low pump levels, the linewidth depicted in Fig. 4c is almost constant, and does not narrow with output power, implying that the linewidth shows no subthreshold behaviour[23,25]. The lack of variation of linewidth with pump power is most likely to be the result of the increasing gain–index coupling, which is a well-known around-threshold behaviour in semiconductor lasers[24,25]. Another indication, and more decisive proof that structure B does not exhibit subthreshold behaviour, is that the linewidth narrowing above the 100 nW pump power level does not follow the inverse power narrowing rate that is clearly identified in structure A. The observed narrowing rate for this laser is attributed to the carrier-pinning effect, as further corroborated by the results of the rate-equations model for the carrier density presented in Supplementary Fig. 13. To the best of our knowledge, this linewidth behaviour, though predicted in theory[26–28], has never been reported in any laser, and is unique to our thresholdless laser. The light–light curve obtained from the rate-equation model for the laser of structure B at 4.5 K is shown by the solid curve in **a** is the best fit of the rate-equation model. The resolution of the monochromator was set to 1.6 nm.

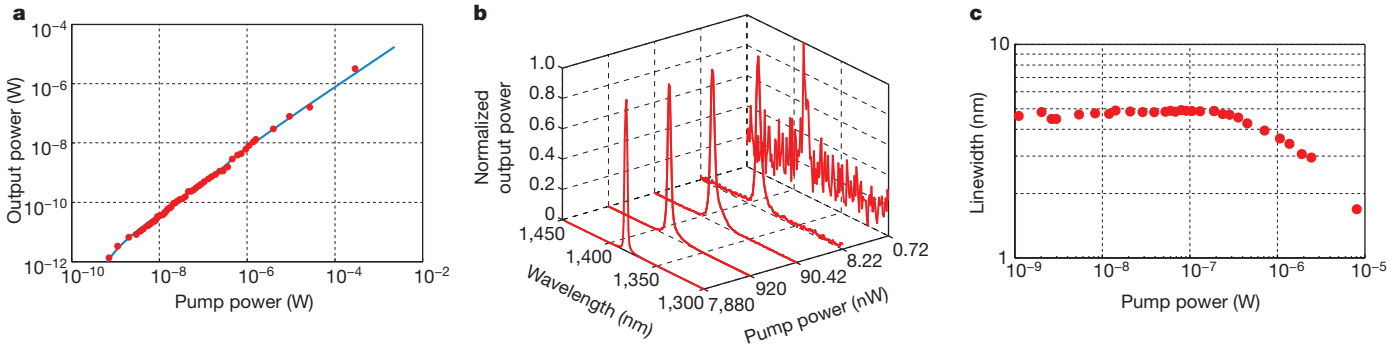

Figure 4 | Optical characterization of nanoscale coaxial cavities of structure B at 4.5 K, showing thresholdless lasing. **a**, Light–light curve; **b**, spectral evolution; and **c**, linewidth evolution. The pump power is calculated as in Fig. 3;

the solid blue line in Fig. 4a. The best fit of our rate-equation model to the experimental data is achieved if 95% of the spontaneous emission is coupled to the lasing mode ($\beta = 0.95$). The deviation from $\beta = 0.99$ predicted by the electromagnetic simulation can be attributed to other non-radiative recombination processes that have not been considered in the rate-equation model, and to the spectral shift of the mode at higher pump levels that causes variations in the available gain for the mode. In summary, all the experimental observations, including output spectrum and beam profile, electromagnetic simulations, rate-equation model, and comparison with the non-thresholdless lasers, suggest thresholdless lasing as the only plausible hypothesis that satisfactorily explains all aspects of the emission of the light-emitting device based on structure B at 4.5 K.

The thresholdless lasing in nanoscale coaxial cavities clearly differs from the state-of-the-art, high-quality-factor, photonic-bandgap structures[29]. In the latter, near-thresholdless lasing is achieved in a quantum dot gain-medium system with spectrally narrow band emission, and relies extensively on tuning of the cavity mode to the centre of the quantum dot emission spectrum[29]. In the former, thresholdless lasing in a broadband gain medium is achieved with a low-quality-factor, single-mode metal cavity. Smaller size, straightforward fabrication procedure, and better thermal properties are just a few of the advantages of nanoscale coaxial cavities for the realization of thresholdless lasing.

In conclusion, with nanoscale coaxial structures, we have successfully demonstrated room-temperature, continuous-wave lasing, as well as low-temperature thresholdless lasing in a spectrally broadband semiconductor gain medium. Owing to the fundamental TEM-like mode with no cut-off, these cavities support ultra-small modes, offer large mode-emitter overlap that results in optimal utilization of the pump power, and provide multifold scalability. Further developments towards electrical pumping of thresholdless nanoscale coaxial lasers that can operate at room temperature are in progress.

The implications of our work are threefold. First, the demonstrated nanoscale coaxial lasers have a great potential for future nano-photonic circuits on a chip. Second, thresholdless operation and scalability provide the first systematic approach toward the realization of QED objects and functionalities, specifically the realization of quantum metamaterials. Last, this new family of resonators paves the way to in-depth study of the unexplored physics of emitter–field interaction, photon statistics, and carrier dynamics in ultra-small metallic structures.

METHODS SUMMARY

Device fabrication. The devices are fabricated on an InP wafer, with 300 μm InP substrate, 200 nm total height of quantum wells, and covered by a 10-nm-thick InP over-layer. Hydrogen silsesquioxane (HSQ) is used as a negative tone resist, on which rings with different inner radii and widths are written by electron beam exposure. The exposed HSQ serves as a mask for the subsequent reactive ion etching (RIE) process that utilizes H_2:CH_4:Ar plasma to remove InGaAsP and InP. The wafer is cleaned with oxygen plasma, and an alloy of silver and aluminium (98%Ag+2%Al) is deposited, using electron-beam evaporation. The sample is mounted on a silicon wafer with silver epoxy, and is dipped in hydrochloric acid to remove the InP substrate.

Material constants. For the finite element method simulation of devices operating at 4.5 K, we used $\varepsilon_{silver} = -120.43 - 0.03073i$ for silver permittivity, $\varepsilon_g = 11.15$ for gain-medium permittivity, $\varepsilon_{InP} = 9.49$ for InP permittivity, $\varepsilon_{SiO2} = 2.1$ for SiO_2 permittivity, and $\varepsilon_{air} = 1$ for air permittivity. For room temperature, the permittivities are the same as at $T = 4.5$ K, except $\varepsilon_{silver} = -120.43 - 3.073i$, $\varepsilon_g = 11.56$ and $\varepsilon_{InP} = 9.86$.

Device measurement. The devices are optically pumped with a 1,064-nm laser beam, focused to an area of ~64 μm^2 on the sample surface. A microscope objective with a numerical aperture of 0.4 is used to focus the pump beam and to collect the output emission. The devices are examined under both continuous wave (CW) and pulsed mode pumping (12-ns pulse width at 300-kHz repetition rate) conditions. Output spectra were obtained using a monochromator with a resolution set at 3.3 nm. When necessary, the linewidth is measured with monochromator resolution set to 1.65 nm and 0.67 nm. The cryogenic measurements were obtained by placing the devices in a continuous-flow microscopy cryostat, and then cooling them with liquid helium to a temperature of 4.5 K.

Received 19 August 2011; accepted 4 January 2012.

1. Berman, P. (ed.) *Cavity Quantum Electrodynamics* (Academic, 1994).
2. Noda, S. Seeking the ultimate nanolaser. *Science* **314,** 260–261 (2006).
3. McCall, S. L., Levi, A. F. J., Slusher, R. E., Pearton, S. J. & Logan, R. A. Whispering-gallery mode microdisk lasers. *Appl. Phys. Lett.* **60,** 289–291 (1992).
4. Painter, O. *et al.* Two-dimensional photonic band-gap defect mode laser. *Science* **284,** 1819–1821 (1999).
5. Hill, M. T. *et al.* Lasing in metallic-coated nano-cavities. *Nature Photon.* **1,** 589–594 (2007).
6. Walther, C., Scalari, G., Amanti, M. I., Beck, M. & Faist, J. Microcavity laser oscillating in a circuit-based resonator. *Science* **327,** 1495–1497 (2010).
7. Mizrahi, A. *et al.* Low threshold gain metal coated laser nanoresonators. *Opt. Lett.* **33,** 1261–1263 (2008).
8. Nezhad, M. P. *et al.* Room-temperature subwavelength metallo-dielectric lasers. *Nature Photon.* **4,** 395–399 (2010).
9. Yu, K., Lakhani, A. & Wu, M. C. Subwavelength metal-optic semiconductor nanopatch lasers. *Opt. Express* **18,** 8790–8799 (2010).
10. Ding, Q., Mizrahi, A., Fainman Y. & Lomakin, V. Dielectric shielded nanoscale patch laser resonators. *Opt. Lett.* **36,** 1812–1814 (2011).
11. Noginov, M. A. *et al.* Demonstration of a spaser-based nanolaser. *Nature* **460,** 1110–1112 (2009).
12. Oulton, R. F. *et al.* Plasmon lasers at deep subwavelength scale. *Nature* **461,** 629–632 (2009).
13. Burgos, S. P., deWaele, R., Polman, A. & Atwater, H. A. A single-layer wide-angle negative-index metamaterial at visible frequencies. *Nature Mater.* **9,** 407–412 (2010).
14. Jacob, Z. & Shalaev, V. M. Plasmonics goes quantum. *Science* **334,** 463–464 (2011).
15. Vahala, K. J. Optical microcavities. *Nature* **424,** 839–846 (2003).
16. Yokoyama, H. Physics and device applications of optical microcavities. *Science* **256,** 66–70 (1992).
17. Bjork, G. & Yamamoto, Y. Analysis of semiconductor microcavity lasers using rate equations. *IEEE J. Quantum Electron.* **27,** 2386–2396 (1991).
18. Baida, F. I., Belkhir, A. & Van Labeke, D. Subwavelength metallic coaxial waveguides in the optical range: Role of the plasmonic modes. *Phys. Rev. B* **74,** 205419 (2006).
19. Feigenbaum, E. & Orenstein, M. Ultrasmall volume plasmons, yet with complete retardation effects. *Phys. Rev. Lett.* **101,** 163902 (2008).
20. Benzaquen, R. *et al.* Alloy broadening in photoluminescence spectra of $Ga_xIn_{1-x}As_yP_{1-y}$ lattice matched to InP. *J. Appl. Phys.* **75,** 2633–2639 (1994).
21. Bayer, M. *et al.* Inhibition and enhancement of the spontaneous emission of quantum dots in structured microresonators. *Phys. Rev. Lett.* **86,** 3168–3171 (2001).
22. Vuckovic, J., Painter, O., Xu, Y., Yariv, A. & Scherer, A. Finite-difference time-domain calculation of the spontaneous emission coupling factor in optical microcavities. *IEEE J. Quantum Electron.* **35,** 1168–1175 (1999).
23. Schawlow, A. L. & Townes, C. H. Infrared and optical masers. *Phys. Rev.* **112,** 1940–1949 (1958).
24. Henry, C. Theory of the linewidth of semiconductor lasers. *IEEE J. Quantum Electron.* **18,** 259–264 (1982).
25. Björk, G., Karlsson, A. & Yamamoto, Y. On the linewidth of microcavity lasers. *Appl. Phys. Lett.* **60,** 304–306 (1992).
26. Rice, P. R. & Carmichael, H. J. Photon statistics of a cavity-QED laser: a comment on the laser-phase-transition analogy. *Phys. Rev. A* **50,** 4318–4329 (1994).
27. Pedrotti, L. M., Sokol, M. & Rice, P. R. Linewidth of four-level microcavity lasers. *Phys. Rev. A* **59,** 2295–2301 (1999).
28. Roy-Choudhury, K. & Levi, A. F. J. Quantum fluctuations and saturable absorption in mesoscale lasers. *Phys. Rev. A* **83,** 043827 (2011).
29. Strauf, S. *et al.* Self-tuned quantum dot gain in photonic crystal lasers. *Phys. Rev. Lett.* **96,** 127404 (2006).
30. Chang, S. W. & Chuang, S. L. Fundamental formulation for plasmonic nanolasers. *IEEE J. Quantum Electron.* **45,** 1014–1023 (2009).

Supplementary Information is linked to the online version of the paper at www.nature.com/nature.

Acknowledgements We acknowledge support from the Defense Advanced Research Projects Agency (DARPA), the National Science Foundation (NSF), the NSF Center for Integrated Access Networks (CIAN), the Cymer Corporation and the US Army Research Office. M. Khajavikhan thanks the personnel of the UCSD Nano3 facilities for their help and support, T. Javidi and J. Leger for technical discussions regarding the analysis of the data and profile of the beam, and graduate student J. Shane for her help with editing the document.

Author Contributions M. Khajavikhan conceived the idea of thresholdless laser using nanoscale coaxial structures. The electromagnetic design, simulation, and analysis of the structures were carried out by M. Khajavikhan, A.M. and V.L. Fabrication of the devices was carried out by M. Khajavikhan and J.H.L. The optical measurements were performed by A.S. and M. Khajavikhan. The rate equation model was developed by M. Katz. The optical characterization and analysis of laser behaviour was carried out by M. Khajavikhan, M. Katz, A.M., B.S. and Y.F. The manuscript was written by M. Khajavikhan, with contributions from A.M., M. Katz, Y.F., A.S., B.S. and V.L.

Author Information Reprints and permissions information is available at www.nature.com/reprints. The authors declare no competing financial interests. Readers are welcome to comment on the online version of this article at www.nature.com/nature. Correspondence and requests for materials should be addressed to M. Khajavikhan (mercedeh@umn.edu).